Research on Chemical Intermediates
https://doi.org/10.1007/s11164-018-03730-y

Synthesis and evaluation of some new hydrazones as corrosion inhibitors for mild steel in acidic media

Hassane Lgaz[1] · **Abdelkarim Chaouiki**[2] · **Mustafa R. Albayati**[3] · **Rachid Salghi**[2] · **Yasmina El Aoufir**[4] · **Ismat H. Ali**[5] · **Mohammad I. Khan**[6] · **Shaaban K. Mohamed**[7,8] · **Ill-Min Chung**[1]

Received: 26 July 2018 / Accepted: 29 December 2018
© Springer Nature B.V. 2019

Abstract

Mild steel corrosion in HCl solution is an example of corrosion in acidic mediums. The ongoing research efforts to develop novel environmentally friendly corrosion inhibitors raise questions regarding their ability to effectively protect steel from corrosion. Herein, a series of experimental studies were conducted to explain the scientific mechanism of adsorption of four hydrazone derivatives (HDZs) namely, 2-((2,3-dimethylphenyl)amino)-*N*′-((1E,2E)-3-phenylallylidene)benzohydrazide (HDZ^1) (E)-2-((2,3-dimethylphenyl)amino)-*N*′-(4-hydroxybenzylidene)benzohydrazide (HDZ^2) (E)-2-((2,3-dimethylphenyl)amino)-*N*′-(1-phenylethylidene)benzohydrazide (HDZ^3) and *N*′-cyclohexylidene-2-((2,3-dimethylphenyl)amino)benzohydrazide (HDZ^4) on mild steel (MS) in 1.0 M HCl using chemical, electrochemical and surface characterization techniques. All results show that the inhibitor molecules form a stable layer on steel surface through chemical and physical interactions. HDZs adsorption onto the steel surface was found to follow Langmuir model. Furthermore, electrochemical results demonstrated that our developed inhibitors act as mixed-type inhibitors, with HDZ^1 showing the highest polarization resistance and lowest corrosion current density. X-ray diffraction and scanning electron microscope were used to study corrosion products phases and surface morphology of MS samples. Our findings provide deeper insights into understanding the interaction mechanisms of HDZs with a steel surface and can be helpful to explore novel approaches to mitigate the steel dissolution.

Keywords Mild steel · Corrosion inhibition · HCl · Hydrazone derivative · Mefenamic acid

---

Electronic supplementary material The online version of this article (https://doi.org/10.1007/s11164-018-03730-y) contains supplementary material, which is available to authorized users.

✉ Ill-Min Chung
imcim@konkuk.ac.kr

Extended author information available on the last page of the article

Published online: 08 January 2019

Introduction

Petroleum refining and related industries which produce multiple fuels and products from petroleum are very important and essential to the function of society. Much of this infrastructure, especially, oil and gas pipelines are made from mild steel. Acidic conditions are widely used in industry for cleaning, descaling, pickling and oil well acidizing. In fact, the corrosion phenomenon for various metals is especially prominent in these industries processes [1–3]. Therefore, the search for chemical substances that can slow down the corrosion rate is a never-ending task. Over several years, much attention has been devoted to the design, synthesis and evaluation of a large number of compounds containing heterocyclic units for potential use as corrosion inhibitors [4–6]. However, very little research has been done so far using hydrazone derivatives on the inhibition of corrosion. Hydrazones are important compounds possessing a wide spectrum of biological and pharmacological properties [7]. Owing to their unique physical and chemical properties, they have been reported to possess potent antimicrobial, analgesic, antifungal, anti-inflammatory and antitumoral activities [8]. On the other hand, Mefenamic acid (MA), a non-steroidal Anti-Inflammatory Drug (NSAID), is well known as one of the most common drugs to the treatment of mild to moderate pain along with other diseases [9, 10]. Functionalization of the free carboxylic group in MA like other NSAIDs could control the most effective side effect of these drugs such as gastrointestinal toxicity [11]. One of the most effective functionalization of carboxylic group is the conversion into hydrazone derivatives [12]. In addition to the advantage of having a MA, the hydrazones are known to exhibit both hard and soft base characters which can facilitate donor–acceptor interactions with electron deficient metal centres. Thus, this synthetic approach can be very useful in the development of effective compounds and satisfy the ever-increasing requirements of the environmental regulation.

This research work is an attempt to develop a better insight and understanding of mechanisms related to corrosion inhibition process of mild steel in 1.0 M HCl using four hydrazone derivatives incorporated Mefenamic acid sub-structure, namely, 2-((2,3-dimethylphenyl)amino)-*N*′-((1E,2E)-3-phenylallylidene)benzohydrazide (HDZ^1), (E)-2-((2,3-dimethylphenyl)amino)-*N*′-(4-hydroxybenzylidene)benzohydrazide (HDZ^2), (E)-2-((2,3-dimethylphenyl)amino)-*N*′-(1-phenylethylidene)benzohydrazide (HDZ^3) and *N*′-cyclohexylidene-2-((2,3-dimethylphenyl)amino)benzohydrazide (HDZ^4) which may provide a platform for further investigations of structurally similar compounds. To the best of our knowledge, no such research has been conducted and this rarity prompted to report the case. We probed the interaction between hydrazone derivatives and the steel surface in 1.0 M HCl using chemical, electrochemical, X-ray diffraction (XRD) and scanning electron microscope (SEM) studies.

Materials and methods

Synthesis

Melting points were recorded using Stuart melting point apparatus. The IR spectra were measured using FTIR spectrometer (Shimadzu, Japan). The ^{1}H NMR and ^{13}C NMR spectra were recorded with Bruker (Bruker 400 MHz; Bruker, Billerica, USA) in DMSO. Scheme 1 represents the general procedure for synthesis of hydrazones (3a–d).

Synthesis and characterization of methyl 2-[(2,3-dimethylphenyl)amino]benzoate (1) A mixture of (2.0 gm, 8.28 mmol) Mefenamic acid and (2.0 gm, 16.6 mmol) anhydrous potassium carbonate was added to dry acetone (80 ml) and stirred for 1 h. Excess of Methyl Iodide (3.6 gm, 24.8 mmol) then added. The resulting mixture was refluxed for 18 h. The reaction mixture was filtered when hot and the resultant cakes were washed with dry acetone (6 × 2 ml). The filtrate was evaporated under reduced pressure to afford the ester as an oily material solidified after 4 days at room temperature with m.p = 100–102 °C (reported [13] 102–103 °C). IR (KBR): (C=O ester 1725 cm^{-1}), (NH$_3$ 332 cm^{-1}), (C–H aliphatic 2999–2943 cm^{-1}), (=C–H aromatic 3012 cm^{-1}).

Synthesis and characterization of 2-[(2,3-dimethylphenyl)amino]benzohydrazide (2) A mixture of Mefenamic acid methyl ester (1) (1 mmol) and hydrazine hydrate (85%, 2.5 mmol) was irradiated, in closed vessel, under microwave irradiation at 300 W and 2500 °C for 7 min. The reaction mixture was cooled, the separated solid

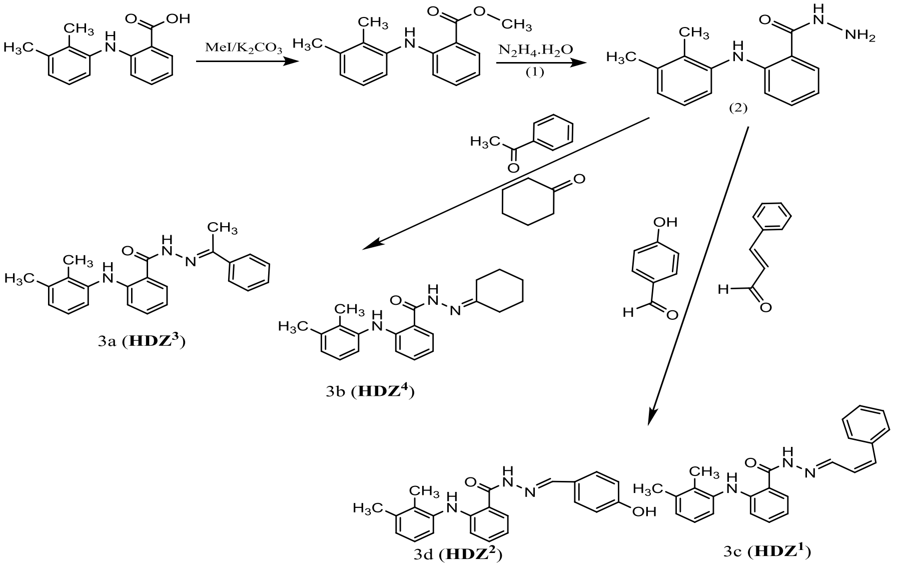

Scheme 1 Hydrazones synthesis scheme

was washed with water, filtered, dried and recrystallized from ethanol to afford the hydrazide (2) with m.p = 119–121 °C (reported [14] 118–120 °C). IR(KBR): (C=O amide 1654 cm^{-1}), (NH 3290 cm^{-1})(NH$_2$,3290–3309 cm^{-1}), (C–H aliphatic 2949), (=C–H aromatic 3018 cm^{-1}). ^{1}H NMR (400 MHz, DMSO): $\delta = 2.1$(s,3H,CH$_3$), 2.2(s,3H,CH$_3$), 9.4(s,1H,NH), 9.8(br.s,1H,NH amide), 3.5(br.s,2H,-NH$_2$), 6.7–7.9(m,7H,Ar–H). ^{13}C-NMR $\delta = 13.5$(CH$_3$), 20.2(CH$_3$), 113.9, 115.9, 116.9, 119.6, 125.0, 125.8, 128.2,129.3,131.8, 137.7,139.3,145.9 (Aromatic carbons),168.4 (C=O amide).

General procedure for synthesis of hydrazones (3a–d) [11] An equimolar mixture of appropriate aldehydes or ketones (0.01 mmol) and mefenamic acid hydrazide 2 (0.01 mmol) with few drops of glacial acetic acid in 25 ml of absolute ethanol was refluxed for 4–5 h. The reaction was concentrated and cooled to half and the solid that precipitated was collected and recrystallized from ethanol to afford 3a–d.

2-[(2,3-dimethylphenyl)amino]-*N*′-[(1E)-1-phenylethylidene] benzohydrazide (3a, $C_{23}H_{23}N_3O$) m.p = 185–188 °C; IR(KBR): (C=O amide 1660 cm^{-1}), (C–H aliphatic 2830 cm^{-1}), (C–H aromatic 3029 cm^{-1}), (NH 3260 cm^{-1})(NH 3193 cm^{-1}), (C=N 1604 cm^{-1}). ^{1}H NMR (400 MHz, DMSO): $\delta = 2.1$(s,3H,CH$_3$), 2.2(s,3H,CH$_3$), 2.3(s,3H,CH$_3$), 9.2(s,1H,NH), 11.8(s,1H,NH amide), 6.7–8.3(m,12H,aromatic).

***N*′-cyclohexylidene-2-[(2,3-dimethylphenyl)amino]benzohydrazide (3b, $C_{21}H_{25}N_3O$)** m.p = 201–203 °C; IR(KBR): (C=O amide 1666 cm^{-1}), (C–H aliphatic 2867–2952 cm^{-1}), (C–H aromatic 3035 cm^{-1}), (NH 3178 cm^{-1})(NH 3123 cm^{-1}), (C=N 1607 cm^{-1}). ^{1}H NMR (400 MHz, DMSO): $\delta = 2.1$(s,3H,CH$_3$), 2.2(s,3H,CH$_3$), 1.1–2.4(m, 10H, aliphatic), 9.2(s,1H,NH),10.3(s,1H,NH amide),6.6–7.6(m,7H,aromatic).

***N*′-[(1E,2E)-3-phenylprop-2-en-1-ylidene]-2-(2,3-dimethylanilino) benzohydrazide (3c, $C_{24}H_{23}N_3O$)** m.p = 206–210 °C; IR(KBR): (C=O amide 1650 cm^{-1}),(NH 3256 cm^{-1})(NH 3125 cm^{-1}), (FC=N 1620 cm^{-1}). ^{1}H NMR (400 MHz, DMSO): $\delta = 2.1$(s,3H,CH$_3$), 2.2(s,3H,CH$_3$), 9.2(s,1H,NH), 10.4(s,1H,NH amide), 6.7–7.9(m,14H,aromatic and –CH=CH– two protons), 7.8(s,1H, –CH=N–). ^{13}C-NMR $\delta = 13$(CH$_3$), 20(CH$_3$), 111–147 (18 Aromatic carbons and –CH=CH– two carbons), 165(C=O amide), 162(C=N).

2-[(2,3-dimethylphenyl)amino]-*N*′-[(E)-(4-hydroxyphenyl)methylidene] benzohydrazide (3d, $C_{22}H_{21}N_3O_2$) m.p = 188–191 °C; IR(KBR): (C=O amide 1655 cm^{-1}), (NH 3115 cm^{-1})(NH 3290 cm^{-1}), (C–H aliphatic 2939 cm^{-1}), (C=N 1613 cm^{-1}). ^{1}H-NMR (400 MHz, DMSO): $\delta = 2.07$ (s,3H,CH$_3$), 2.2(s, 3H,CH$_3$), 9.2(s,1H,NH), 10.2(s,1H,NH), 11.9(sb,1H,OH), 6.7–7.5(m,11H,aromatic), 7.8(s,1H, –CH=N–). ^{13}C-NMR $\delta = 13$(CH$_3$), 20.08(CH$_3$), 111–147(18 aromatic carbons), 162(C=N), 165(C=O amide).

Mild steel samples and corrosive solutions

The chemical composition in mass percent (wt%) of metal substrates used in the research was: 0.36 C, 0.66 Mn, 0.27 Si, 0.02 S, 0.015 P, 0.21 Cr, 0.02 Mo, 0.22 Cu, 0.06 Al, and balance Fe. The mild steel samples were mechanically abraded with a series of emery papers (400–1600 grades) and cleaned thoroughly. The stock solutions were prepared by diluting 37% analytical grade HCl with double distilled water.

Weight loss measurements

All the experimental procedures including the shape and size of mild steel specimens were based on the ASTM standard [15]. In essence, mild steel samples were immersed in uninhibited and inhibited solutions for 24 h at 303 K. The samples were prepared as mentioned previously and weighted using a precision balance with a sensitivity of 0.1 mg. After each test, MS specimens were taken out and rinsed thoroughly with distilled water and acetone, dried and weighted accurately again. The experiments were carried out in triplicates and only the average values of weight losses were reported.

Electrochemical measurements

The electrochemical measurements were performed in a conventional three-electrode cell kit using Volta Lab (Tacussel-Radiometer PGZ 100) potentiostat. The three-electrode system consisted of a working electrode (mild steel) with the surface area of 1 cm^2 in contact with the electrolyte, Pt as an auxiliary electrode alongside a saturated calomel reference electrode. Before electrochemical measurements, the working electrode was first immersed in the test solution for 30 min in order to be in equilibrium with the environment. Measurement of the impedance spectra was obtained in the frequency range of 10 mHz to 100 kHz and an AC amplitude of 5 mV. The Tafel polarization measurements were recorded at a scanning rate of 1 mV s^{-1} in the range from -800 to -200 mV versus SCE relative to the corrosion potential. All electrochemical measurements were performed in a cell containing 80 mL of the electrolyte at 303 K.

SEM and XRD studies

The surface morphology and corrosion products phases of mild steel samples were characterized with scanning electron microscopy and XRD in the absence and presence of 5×10^{-3} M of inhibitors. SEM imaging and XRD analyses were performed on samples after a 24 h immersion time. A Hitachi TM-1000 SEM at an accelerating voltage of 15 kV and Bruker D8 powder diffractometer with CuKα radiation (λCu = 1.5407 Å) were used for SEM and XRD analyses.

Results and discussion

Weight loss measurements

We performed gravimetric tests to explore the effects of different amounts of hydrazone derivatives on the corrosion rate of mild steel in 1.0 M HCl. The following Eq. (1) was used to determine the corrosion rate in millimeters per year (mm year^{-1}) [16]:

$$C_{\mathrm{RW}} = \frac{K \times W}{A \times t \times \rho} \tag{1}$$

here $K = 8.76 \times 10^4$ was used as constant. *W*, *t and A* are the mass loss in gram, the time of exposure in hours and the exposed area in cm^2 [17], respectively. The density of carbon steel is 7.86 g cm^{-3}. The values of the inhibition efficiency, $\eta_{\mathrm{WL}}(\%)$, are calculated using the following equation [16]:

$$\eta_{\mathrm{WL}}(\%) = \frac{C_{\mathrm{R}} - C_{\mathrm{R}}^{\circ}}{C_{\mathrm{R}}} \times 100 \tag{2}$$

where C_{R} and C_{R}° are corrosion rates before and after the addition of hydrazone derivatives, respectively.

The results derived from gravimetric tests are summed up in Table S1 (Supplementary information (SI)) and Fig. 1. The results in Fig. 1 indicate that for all hydrazone derivatives, the addition of small amounts of inhibitors in 1.0 M HCl did not

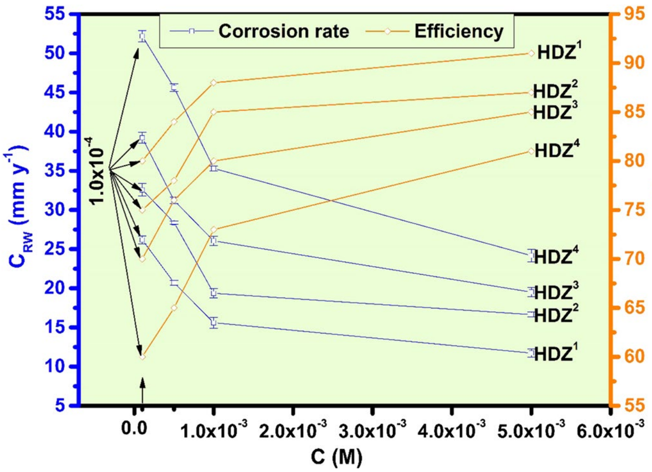

Fig. 1 Variation of inhibition efficiency and corrosion rate with inhibitor concentration at 303 K

significantly decrease the corrosion rate. In contrast, the inhibitive effect was more pronounced at a higher concentration. As the concentration of inhibitor increased, more inhibitive activity could be gained in a concentration-dependent manner. The most likely explanation of these results is that at higher concentrations, inhibitor molecules may have a strong ability to interact with iron atoms, and by increasing concentrations, more and more inhibitor molecules enter double layer level by replacing preexisting water molecules [18–21]. The hydrazone derivatives were found to attain the maximum $\eta_{WL}(\%)$ at 5×10^{-3} M whereas the efficiency of adsorption was at the order $HDZ^1 > HDZ^2 > HDZ^3 > HDZ^4$. These results are addressed in more detail in the next sections.

Electrochemical studies

Electrochemical studies provide unique valuable information about the response of mild steel samples exposed to corrosion conditions and the possible influence of inhibitors on corrosion resistance. The polarization measurements (Tafel plots) collected during the experiments are graphically represented in Fig. 2. The main electrochemical parameters such as corrosion current density (i_{corr}) corrosion potential (E_{corr}), cathodic and anodic Tafel slopes (β_c, β_a) along with the corresponding inhibition efficiency were determined and tabulated in Table 1.

Note that only results of optimum concentration are reported, and full electrochemical results are available in SI Figures S1-S3 and Tables S2 and S3. The inhibition efficiency ($\eta_{PDP}(\%)$) is calculated using [16]:

$$\eta_{PDP}(\%) = \left[1 - \frac{i_{corr}}{i^{\circ}_{corr}}\right] \times 100 \tag{3}$$

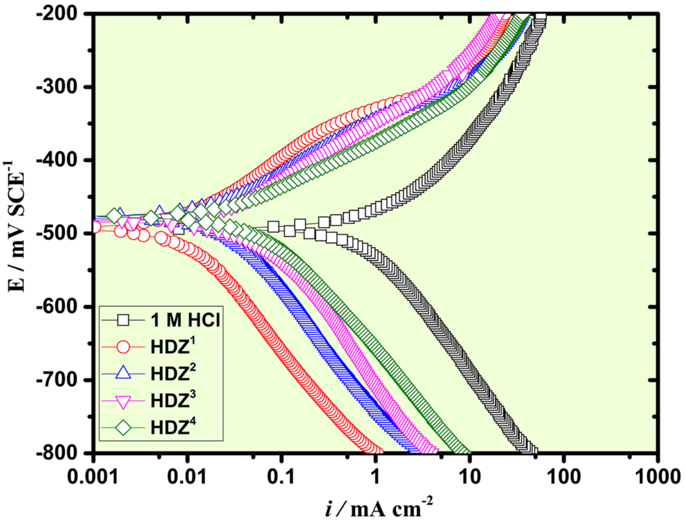

Fig. 2 Polarization curves for mild steel in 1.0 M HCl and in presence of hydrazone derivatives at 303 K

Table 1 The parameters of PDP of the mild steel in uninhibited and inhibited solutions at 303 K

Inhibitors	Concentration (M)	$-E_{corr}$ (mV vs. SCE)	$-\beta_c$ (mV dec^{-1})	β_a (mV dec^{-1})	i_{corr} (μA cm^{-2})	η_{PDP} (%)
Uninhibited	–	496	150	92	597	–
HDZ^1	5×10^{-3}	493	174	59	28	95
HDZ^2	5×10^{-3}	480	144	63	48	92
HDZ^3	5×10^{-3}	483	154	69	76	87
HDZ^4	5×10^{-3}	478	140	70	94	84

In this equation, i°_{corr} corresponds to the corrosion current density under uninhibited solutions, and i_{corr} is the corrosion current density in presence of inhibitor obtained by extrapolation of the Tafel lines.

After adding the different concentrations of hydrazone derivatives, we observed decreased current densities in both anodic and cathodic branches as expected. This effect became more pronounced as a function of increasing inhibitor concentration, suggesting that many of the active surface sites were blocked due to the adsorption of inhibitor molecules. Moreover, the results showed that the corrosion potential values remained nearly in the same range in the presence of all inhibitors concentrations suggesting that HDZs are mixed type corrosion inhibitors [22]. We can also observe from the Fig. 2 that all cathodic branches decreased markedly to lower values and give rise to parallel lines indicating that inhibitors molecules do not modify the hydrogen evolution mechanism and this reaction is activation controlled [23]. In other words, the reaction mechanism remains unaffected while the surface area available for hydrogen evolution is significantly decreased and the access of H^+ to the mild steel surface became more difficult [24]. In contrast, we observed markedly different effects of the inhibitor molecules on the metal dissolution reaction. At low applied over potentials, a gradual decrease of the mild steel dissolution rate was observed while at higher positive potentials, precisely over −250 mV vs. SCE, a significant reduction in the corrosion resistance was observed. Typically, at low over potentials, a protective layer of adsorbed molecules is formed and when the electrode potential reaches desorption potential, inhibitor molecules adsorbed on the steel surface commence to move away and no longer can sufficiently protect the mild steel at a higher potential than desorption potential [25].

There is no denial that a lower corrosion rate leads to an improved corrosion resistance. Fortunately, useful information to explain performance differences of the different hydrazone derivatives can be obtained from direct electrochemical parameters. As can be seen from Table 1, the addition of inhibitor molecules significantly reduces the corrosion current density values of the inhibited sample. Based on the current data, we can indeed conclude that the order of increase of inhibitive effect of tested hydrazones on steel corrosion is as follows: $HDZ^1 > HDZ^2 > HDZ^3 > HDZ^4$. This result let us to assume that the relative performance of the different inhibitors is determined by their structure, essentially by the number of heteroatoms, the nature of the functional groups, the length of the π-electron system and etc. Polarization measurement results are consistently in good agreement with those from weight loss tests.

Electrochemical impedance spectroscopy results are displayed as Nyquist and Bode plots in Fig. 3. The examination of the results indicates that all Nyquist plots show only one depressed capacitive semicircle and only one-time constant was observed in Bode format. This implies that only one phenomenon occurred, and the charge transfer process is the only effective pathway to control the dissolution of mild steel at the metal/solution interface [26].

The results showed that the impedance response of the mild steel in 1.0 M HCl was significantly affected by adding hydrazone derivatives. As expected, we found that the

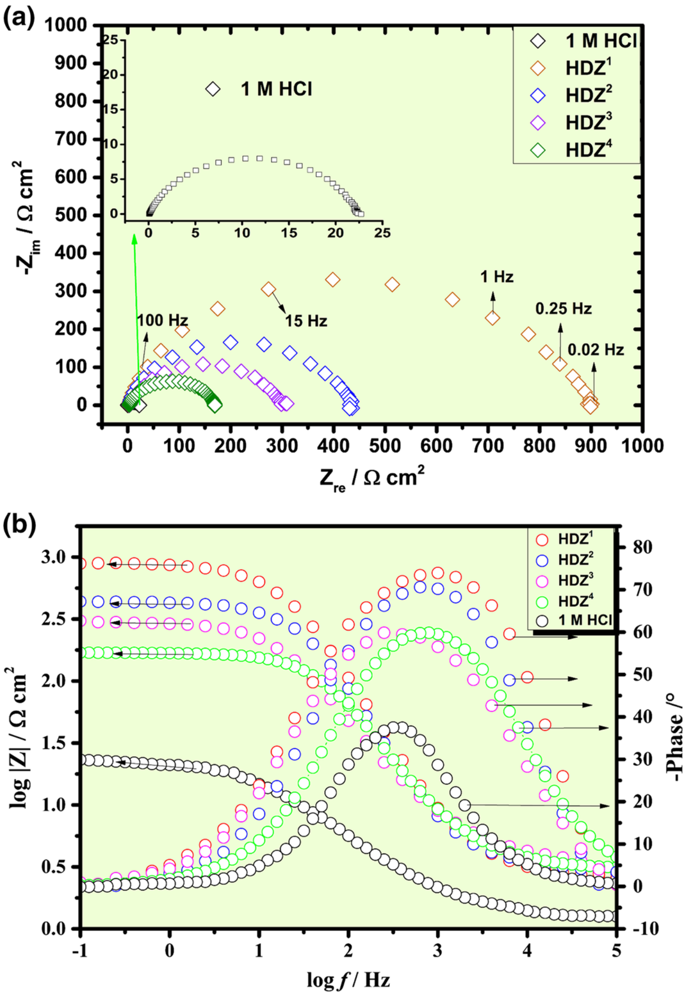

Fig. 3 Impedance results for mild steel in 1.0 M HCl and in presence of hydrazone derivatives at 303 K **a** Nyquist plots, **b** Bode and phase angle plots

diameters of the semicircles increased with the increasing of the HDZs concentration. It is important to note that by increasing the inhibitor concentration, more inhibitor molecules adsorbed on the steel surface, so that a non-conducting protective layer can be formed by an effective replacement of the pre-adsorbed water molecules [27].

Furthermore, we address the evolution of phase angle by measuring their values at arbitrarily chosen frequency (1 kHz) as shown in Fig. 4 (only HDZ^1). Clearly, the phase angle value increased considerably as the inhibitor concentration increased. This indicates increased adsorption of inhibitor molecules which, in turn, permits the formation of a more protective surface layer. The results were also supported by the increase of the absolute impedance at low frequencies in the Bode plots. Furthermore, whatever the concentration used, the angle phase values are higher than that of the blank, but lower than $-90°$, which describes the non-ideal capacitor.

The Nyquist diagrams represented in Fig. 3 are depressed semicircles and not perfect as expected from the theory of EIS, which is a common phenomenon on solid electrodes. Generally, a slight inclination of the impedance plots is frequently observed and it is related to the surface heterogeneity attributed to roughness and inhomogeneities of solid surfaces [28]. To account for this effect, we replace the capacitance of the electric double-layer by a constant phase element (CPE) in the electrical circuit model used to fit the EIS data (Fig. 5). The equivalent circuit model includes a circuit (*R*p//CPE) (polarization resistance in parallel with the CPE) in series with the resistance of the solution.

The CPE formula most often used for adjustment is defined by the following equation [28].

$$Z_{\mathrm{CPE}} = \frac{1}{Q(j\omega)^n} \tag{4}$$

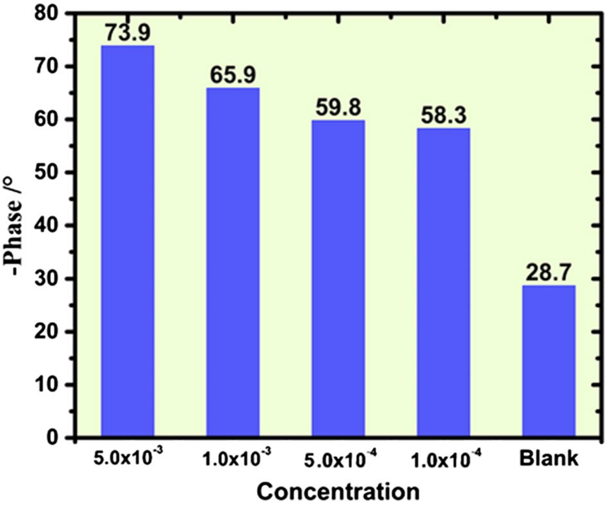

Fig. 4 Phase angle values at 1 kHz for mild steel in 1.0 M HCl in presence of HDZ^1

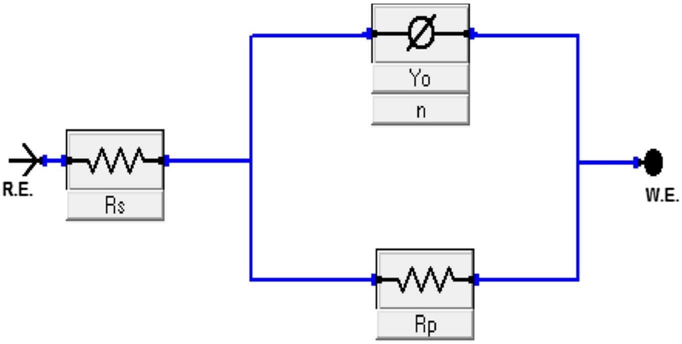

Fig. 5 The electrical circuit model used to fit the EIS data

where Q is the CPE magnitude, ω is the angular frequency, $j^2 = -1$ is the imaginary unit and n the exponential term, which can be associated with the roughness of the metal surface [29]. When n is close to 1, 0 or − 1, the CPE represents a capacitor, a resistance or inductance, respectively. In addition, if $n = 0.5$ the result is equivalent to Warburg diffusion. The CPE is extremely flexible for adjusting impedance diagrams. The double layer capacitance value (C_{dl}) is defined by the following equation [30]:

$$C_{\mathrm{dl}} = \sqrt[n]{Q \times R_{\mathrm{p}}^{1-n}} \tag{5}$$

All electrochemical impedance parameters along with the inhibition efficiency $\eta_{EIS}(\%)$ are listed in Table 2 and S3 (SI). The protection efficiencies were calculated according to Eq. (6):

$$\eta_{\mathrm{EIS}}(\%) = \left[\frac{R_{\mathrm{p(inh)}} - R_{\mathrm{p}}}{R_{\mathrm{p(inh)}}}\right] \times 100 \tag{6}$$

here R_{p} and $R_{\mathrm{p(inh)}}$ represent the polarization resistances of metal coupons in 1.0 M HCl before and after the addition of the inhibitor, respectively.

From Table 2, it is clearly seen that the values of the polarisation resistance in presence of hydrazone derivatives are much higher than that in blank solution which

Table 2 Impedance parameters for corrosion of mild steel in uninhibited and inhibited solutions at 303 K

Inhibitors	Concentration/M	R_s (Ω cm^2)	R_p (Ω cm^2)	n	$Q \times 10^{-4}$ (S^n Ω^{-1} cm^{-2})	C_{dl} (μF cm^{-2})	η_{EIS} (%)
Uninhibited	–	0.08	22.3	0.79	35.340	182	–
HDZ^1	5×10^{-3}	2.50	853.8	0.86	0.1331	6	97
HDZ^2	5×10^{-3}	2.80	419.0	0.81	0.2924	10	94
HDZ^3	5×10^{-3}	2.50	293.0	0.78	0.4872	14	92
HDZ^4	5×10^{-3}	3.10	166.4	0.82	0.7802	30	86

is indicative of decreased metal dissolution reaction. Meanwhile, a marked decrease was observed in the double layer capacitance in presence of inhibitor molecules. This led to changes in the interface indicative of the enhanced adsorption of inhibitors on steel surface, and consequently there had been a large increase in the thickness of the electric double layer. Then, the dissolution of steel efficiently minimized. As much as the substituent of different hydrazone derivatives differs so does differ the impacts on steel/electrolyte interface. Like potentiodynamic polarization and weight loss results, the inhibition performances of tested compounds follow the order of $HDZ^1 > HDZ^2 > HDZ^3 > HDZ^4$.

Adsorption isotherm

Several studies dealing with the interaction between organic compounds and steel surface have revealed that in most instances the inhibitor molecules establish their inhibition via the adsorption onto the metal surface. This adsorption process of inhibitor molecules can be through physical, chemical or physicochemical adsorption. Such information can be typically obtained from the use of adsorption isotherm models [28]. In our study, the experimental data were subjected into various adsorption isotherms such as Langmuir, Temkin, and Frumkin. The Langmuir model was found to provide the best description of inhibitor adsorption. The general equation of this isotherm is [31]:

$$\frac{C}{\theta} = \frac{1}{K_{\mathrm{ads}}} + C \tag{7}$$

The terms shown in the above equation are defined as follow: K_{ads} is the adsorption–desorption equilibrium constant and C_{inh} is the inhibitor concentration. The $\Delta G^{\circ}_{\mathrm{ads}}$ values (free energy of adsorption) were calculated using the following equation [32]:

$$\Delta G^{\circ}_{\mathrm{ads}} = -RT\ln(K_{\mathrm{ads}} \times 55.5) \tag{8}$$

here 55.5 is the concentration of H_2O in solution in mol L^{-1}, R and T are the molar gas constant (8.3144598 J/K) and absolute temperature respectively.

The plot of C/θ versus C gave the best fit (Fig. 6) with R^2 and slope values close to 1 confirming that the adsorption of all hydrazone derivatives on the surface of the mild steel in 1.0 M HCl obeys the Langmuir adsorption isotherm. Importantly, the data in Table 3 suggested that the magnitude of the adsorption free energy and the adsorption–desorption equilibrium constant followed the order of $HDZ^1 > HDZ^2 > HDZ^3 > HDZ^4$. These results indicate that the extent of adsorption of tested compounds varies widely with the corresponding differences in their molecular structures.

The results summarized in Table 3 also indicate that the adsorption free energy values of all compounds are between -40 and -30 kJ mol^{-1}, which indicate the presence of a physical and chemical adsorption of hydrazone derivatives on steel surface [33]. As we mentioned above, there are significant differences

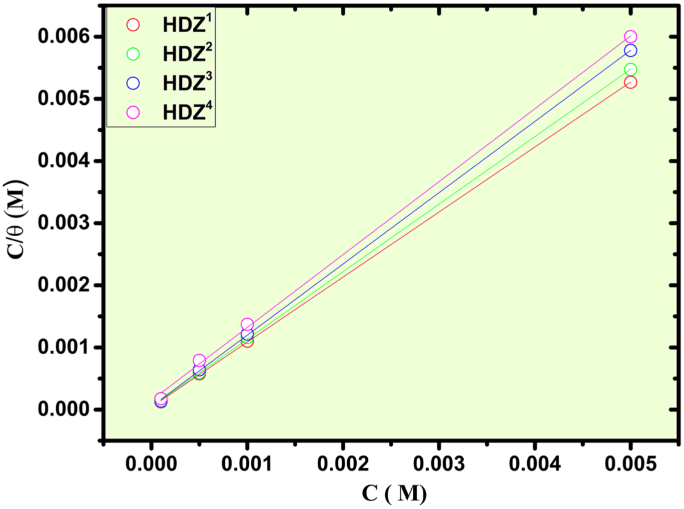

Fig. 6 Langmuir adsorption isotherm for the studied inhibitors on mild steel in 1 M HCl at 303 K

Table 3 The adsorption parameters for the corrosion of MS in inhibited solutions at 303 K

Inhibitors	Slope	K_{ads} (M^{-1})	R^2	ΔG°_{ads} (kJ mol^{-1})
HDZ^1	1.04	24569	0.9997	−35.5
HDZ^2	1.06	21472	0.9995	−35.2
HDZ^3	1.03	19663	0.9998	−35.0
HDZ^4	1.06	6732	0.9995	−32.3

between the tested inhibitor molecules in terms of functional groups, which lead to a different extent of inhibitor adsorption.

SEM study

SEM analysis is a useful tool to characterize the surface morphology of the mild steel samples. The SEM images of the MS samples before and after their immersion in 1.0 M HCl are given in Fig. 7. The results of the SEM imaging in Fig. 7 showed a highly corroded and damaged steel surface, largely due to rapid corrosion attack in acidic solution. Opposite to that, a smoother surface morphology was observed after the addition of hydrazone derivatives, which is mainly attributed to the formation of an adsorption layer thereby decreasing the corrosion effects. Moreover, there are still some traces of scratches and some polishing lines resulting from the steel surface treatment.

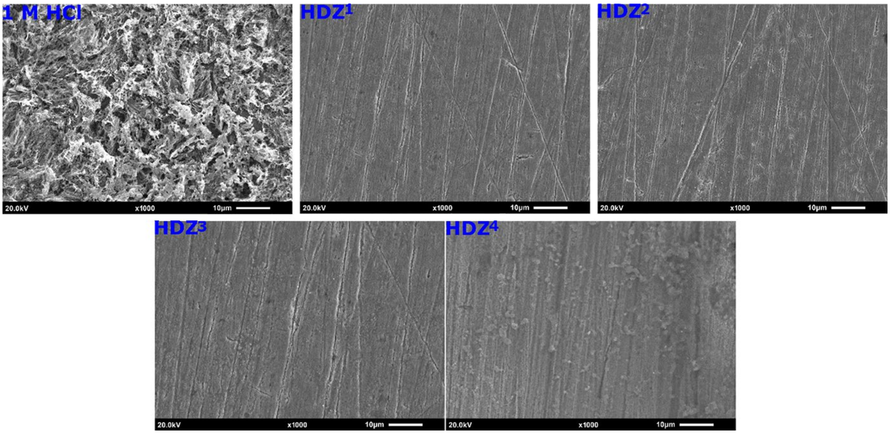

Fig. 7 SEM pictures of mild steel in acid solution and in presence of 5×10^{-3} M HDZs after 24 h immersion time at 303 K

X-ray diffraction analysis

The inhibitory effect of the hydrazone derivatives on the corroded steel surface was displayed through SEM analysis. However, to further address this effect, the samples of polished, corroded (blank) and inhibited mild steel were examined by X-ray diffraction. Figure 8 presents XRD patterns of the three steel samples. In the polished and corroded samples, the diffraction peaks at about 44.6°, 64.6°, and 82.4° were the characteristic peaks of Fe. In addition, the diffraction peaks corresponding to 28.3°, 35.2° and 36.2° were observed in the corroded sample due to the formation of the

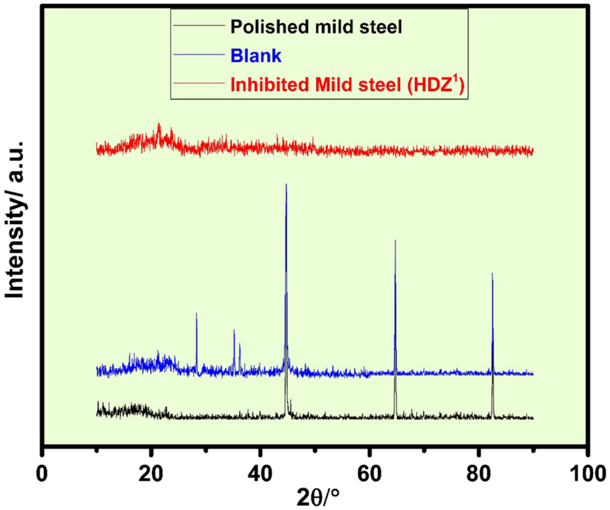

Fig. 8 X-ray diffraction pattern of polished, corroded and inhibited mild steel samples

corrosion products. In contrast, no apparent peaks were observed for the inhibited sample and the corrosion products were mainly suppressed. These results confirm again that the hydrazone derivatives greatly reduce the attack of HCl solution on the steel surface via formation of a protective layer [34].

Anticorrosion mechanism of hydrazone derivatives

Despite the large number of published works on the biological properties of hydrazone derivatives, the studies on the effectiveness and mechanism of these compounds in corrosion inhibition remain insufficient. Herein, this study was designed to address the gaps in knowledge regarding the use of hydrazone derivatives prepared via functionalization of the MA. The results showed that the hydrazone derivatives are effective corrosion inhibitors with great electronic properties. Based on the results we obtained in this study, we propose a mechanism for the interaction of tested hydrazones with steel surface in Fig. 9 taking as example the HDZ^1.

Due to the presence of heteroatoms in the molecular structure of the tested hydrazones, it is thought to have a greater proton affinity. This is also a common feature in many corrosion inhibition studies under acidic environment [35]. In the meantime, the chlorine ions play an important role in the adsorption process of the tested compounds. According to several previous studies examining the corrosion inhibition of mild steel in HCl medium [36–39], the surface of mild steel possesses a negative charge in HCl solution in the presence of inhibitors. Thus, it is assumed that Cl^- ion first get adsorbed onto the positively charged metal surface by columbic attraction and then cationic form of inhibitor molecules can be adsorbed through electrostatic interactions between the positively charged molecules and the negatively charged metal surface. This process can be easily found in our case due to the presence of nitrogen and oxygen atoms in all tested hydrazones. This physisorption process is

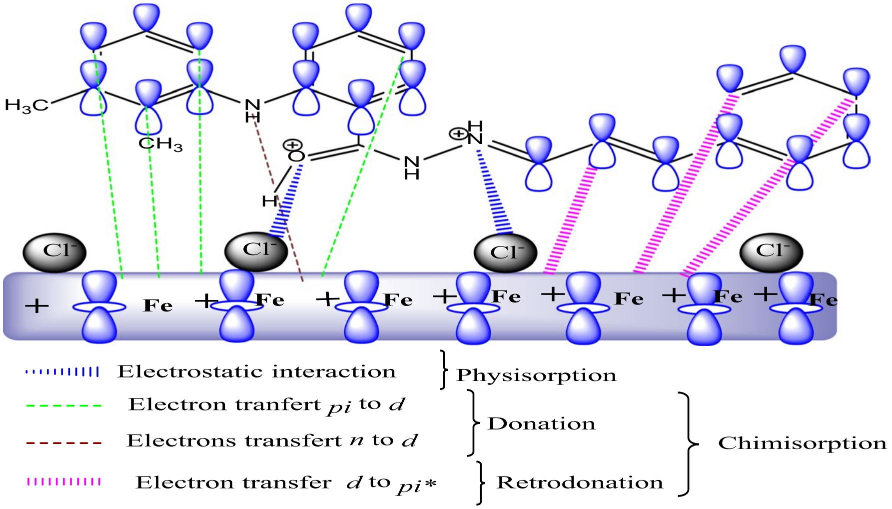

Fig. 9 Pictorial representation of adsorption of HDZ^1 on MS surface in 1.0 M HCl

the first step and the base of chemical adsorption, then, the hydrazone derivatives can be chemically adsorbed through acceptor–donor interactions [40]. The presence of π-electrons of the phenyl rings and unshared electron pairs in heteroatoms can ensure the donation of the electron to the vacant d-orbitals of iron, which is chemical adsorption. Another form of the chemical interaction is what′s known as back-donation of electrons from filled d-orbitals of the iron to empty π-acceptors on organic compounds. The greater amount of the reactive sites will lead to an extra negative charge on steel surface due to the strong donation of electrons which will be transferred to inhibitor molecules by means of back-donation interactions, therefore enhancing the adsorption on the metal surface.

Conclusion

In summary, this work has investigated the inhibition effect of four hydrazone derivatives prepared through functionalization of MA on the mild steel corrosion in 1.0 M HCl. An experimental approach has been done to probe the corrosion inhibition mechanism underlying the effectiveness of these inhibitors. Among tested compounds, the HDZ^1 produces better inhibitive performances. The electrochemical results illustrate that the HDZs behave as mixed type inhibitors; their addition to corrosive solutions leads to a high increase of the polarization resistance and correspondingly lower double-layer capacitance. The information about adsorption mode was extracted from Langmuir adsorption model. These insights seem very important and encourage us to invest in the development of other corrosion inhibitors through functionalization of others NSAID’s. A comprehensive theoretical overview of factors potentially affecting the performance of tested compounds will be reported in future work.

Acknowledgements The authors extend their appreciation to the Deanship of Scientific Research at King Khalid University for funding this work through research groups program under Grant Number R.G.P-1.21-38.

Compliance with ethical standards

Conflict of interest The authors declare that they have no conflict of interest.

References

1. A.K. Singh, E.E. Ebenso, Res. Chem. Intermed. **39**, 1823 (2013)
2. Z. Mohammadi, M. Rahsepar, Res. Chem. Intermed. **44**, 2139 (2018)
3. K. Adardour, R. Touir, Y. Ramli, R.A. Belakhmima, M.E. Touhami, C.K. Mubengayi, H.E. Kafsaoui, E.M. Essassi, Res. Chem. Intermed. **39**, 1843 (2013)
4. I.B. Obot, N.O. Obi-Egbedi, E.E. Ebenso, A.S. Afolabi, E.E. Oguzie, Res. Chem. Intermed. **39**, 1927 (2013)
5. A.K. Singh, S. Khan, A. Singh, S.M. Quraishi, M.A. Quraishi, E.E. Ebenso, Res. Chem. Intermed. **39**, 1191 (2013)
6. B. Fan, H. Hao, B. Yang, Y. Li, Res. Chem. Intermed. **44**, 5711 (2018)
7. S. Rollas, S.G. Küçükgüzel, Molecules **12**, 1910 (2007)

8. G. Verma, A. Marella, M. Shaquiquzzaman, M. Akhtar, M.R. Ali, M.M. Alam, J. Pharm. Bioallied Sci. **6**, 69 (2014)
9. M. Antonio, R.M. Maggio, J. Pharm. Biomed. Anal. **149**, 603 (2018)
10. Y. Joo, H.-S. Kim, R.-S. Woo, C.H. Park, K.-Y. Shin, J.-P. Lee, K.-A. Chang, S. Kim, Y.-H. Suh, Mol. Pharmacol. **69**, 76 (2006)
11. S.K. Mohamed, J.T. Mague, M. Akkurt, A.F. Mohamed, M.R. Albayati, Acta Crystallogr. Sect. E Crystallogr. Commun. **71**, o957 (2015)
12. A. Almasirad, M. Tajik, D. Bakhtiari, A. Shafiee, M. Abdollahi, M.J. Zamani, R. Khorasani, H. Esmaily, J Pharm Pharm Sci **8**, 419 (2005)
13. H. Nawaz, M. Khawar Rauf, M. Ebihara, A. Badshah, Acta Crystallogr. Sect. E: Struct. Rep. Online **63**, o1658 (2007)
14. T. Aboul-Fadl, H.A. Abdel-Aziz, A. Kadi, A. Bari, P. Ahmad, T. Al-Samani, S.W. Ng, Molecules **16**, 3544 (2011)
15. J. Scully, R. Baboian, *Standard Practice for Laboratory Immersion Corrosion Testing of Metals*, vol. 110 (ASTM, Philadelphia, 1995)
16. Z. Salarvand, M. Amirnasr, M. Talebian, K. Raeissi, S. Meghdadi, Corros. Sci. **114**, 133 (2017)
17. ASTM Committee G-1 on Corrosion of Metals, *Standard Practice for Preparing, Cleaning, and Evaluating Corrosion Test Specimens* (ASTM International, West Conshohocken, 2011)
18. A.S. Fouda, T.F. Alsawy, E.S. Ahmed, B.S. Abou-elmagd, Res. Chem. Intermed. **39**, 2641 (2013)
19. S. Belkaid, K. Tebbji, A. Mansri, A. Chetouani, B. Hammouti, Res. Chem. Intermed. **38**, 2309 (2012)
20. A. Singh, J.N. Avyaya, E.E. Ebenso, M.A. Quraishi, Res. Chem. Intermed. **39**, 537 (2013)
21. A. Mansri, B. Bouras, B. Hammouti, I. Warad, A. Chetouani, Res. Chem. Intermed. **39**, 1753 (2013)
22. H. Lgaz, O. Benali, R. Salghi, S. Jodeh, M. Larouj, O. Hamed, M. Messali, S. Samhan, M. Zougagh, H. Oudda, Pharma Chem. **8**, 172 (2016)
23. R. Fuchs-Godec, Colloids Surf. Physicochem. Eng. Asp. **280**, 130 (2006)
24. A. Chetouani, B. Hammouti, T. Benhadda, M. Daoudi, Appl. Surf. Sci. **249**, 375 (2005)
25. F. Bentiss, F. Gassama, D. Barbry, L. Gengembre, H. Vezin, M. Lagrenée, M. Traisnel, Appl. Surf. Sci. **252**, 2684 (2006)
26. H. Lgaz, R. Salghi, M. Larouj, M. Elfaydy, S. Jodeh, Z. Rouifi, B. Lakhrissi, H. Oudda, J. Mater. Environ. Sci. **7**, 4471 (2016)
27. M. Messali, H. Lgaz, R. Dassanayake, R. Salghi, S. Jodeh, N. Abidi, O. Hamed, J. Mol. Struct. **1145**, 43 (2017)
28. S.K. Saha, A. Dutta, P. Ghosh, D. Sukul, P. Banerjee, Phys. Chem. Chem. Phys. **17**, 5679 (2015)
29. H. Lgaz, R. Salghi, S. Jodeh, B. Hammouti, J. Mol. Liq. **225**, 271 (2017)
30. A. Singh, K.R. Ansari, J. Haque, P. Dohare, H. Lgaz, R. Salghi, M.A. Quraishi, J. Taiwan Inst. Chem. Eng. **82**, 233 (2018)
31. K. Toumiat, Y. El Aoufir, H. Lgaz, R. Salghi, S. Jodeh, M. Zougagh, H. Oudda, Res. J. Pharm. Biol. Chem. Sci. **7**, 1209 (2016)
32. L.O. Olasunkanmi, I.B. Obot, E.E. Ebenso, RSC Adv. **6**, 86782 (2016)
33. M. Yadav, S. Kumar, R.R. Sinha, I. Bahadur, E.E. Ebenso, J. Mol. Liq. **211**, 135 (2015)
34. S. Tu, X. Jiang, L. Zhou, M. Duan, H. Wang, X. Jiang, Corros. Sci. **65**, 13 (2012)
35. R. Yıldız, T. Doğan, İ. Dehri, Corros. Sci. **85**, 215 (2014)
36. Z. Cong, W. Li, D. Hu, Z. Lan, B. Hou, Electrochemistry **83**, 262 (2015)
37. P. Han, W. Li, H. Tian, X. Gao, R. Ding, C. Xiong, L. Song, X. Zhang, W. Wang, C. Chen, Mater. Chem. Phys. **214**, 345 (2018)
38. R. Solmaz, Corros. Sci. **81**, 75 (2014)
39. R. Solmaz, E. Altunbaş, G. Kardaş, Mater. Chem. Phys. **125**, 796 (2011)
40. L. Tang, X. Li, L. Li, G. Mu, G. Liu, Mater. Chem. Phys. **97**, 301 (2006)

Publisher's Note Springer Nature remains neutral with regard to jurisdictional claims in published maps and institutional affiliations.

Affiliations

Hassane Lgaz[1] · Abdelkarim Chaouiki[2] · Mustafa R. Albayati[3] · Rachid Salghi[2] · Yasmina El Aoufir[4] · Ismat H. Ali[5] · Mohammad I. Khan[6] · Shaaban K. Mohamed[7,8] · Ill-Min Chung[1]

[1] Department of Crop Science, College of Sanghur Life Science, Konkuk University, Seoul 05029, South Korea

[2] Laboratory of Applied Chemistry and Environment, ENSA, University Ibn Zohr, PO Box 1136, Agadir, Morocco

[3] Department of Chemistry, College of Education, Kirkuk University, Kirkuk, Iraq

[4] Materials, Nanotechnology and Environment Laboratory, Faculty of Sciences, Mohammed V University Rabat, Rabat, Morocco

[5] Department of Chemistry, College of Science, King Khalid University, P. O. Box 9004, Abha 61413, Kingdom of Saudi Arabia

[6] Chemical Engineering Department, College of Engineering, King Khalid University, Abha, Kingdom of Saudi Arabia

[7] Faculty of Science and Engineering, Health Care Division, Manchester Metropolitan University, Manchester, England M1 5GD, UK

[8] Chemistry Department, Faculty of Science, Minia University, El-Minia 61519, Egypt